DFIG Machine Design for Maximizing Power Output Based on Surrogate Optimization Algorithm

Zheng Tan, *Student Member, IEEE*, Xueguan Song, *Member, IEEE*, Wenping Cao, *Senior Member, IEEE*, Zheng Liu, *Student Member, IEEE*, and Yibin Tong

***Abstract*—This paper presents a surrogate-model-based optimization of a doubly-fed induction generator (DFIG) machine winding design for maximizing power yield. Based on site-specific wind profile data and the machine's previous operational performance, the DFIG's stator and rotor windings are optimized to match the maximum efficiency with operating conditions for rewinding purposes. The particle swarm optimization-based surrogate optimization techniques are used in conjunction with the finite element method to optimize the machine design utilizing the limited available information for the site-specific wind profile and generator operating conditions. A response surface method in the surrogate model is developed to formulate the design objectives and constraints. Besides, the machine tests and efficiency calculations follow IEEE standard 112-B. Numerical and experimental results validate the effectiveness of the proposed technologies.**

***Index Terms*—Doubly fed induction generator, operating conditions, particle swarm optimization, power loss, rewinding, surrogate model, wind power generation.**

I. Introduction

WITH THE increasing concern over global warming and the depletion of fossil fuels, the development of renewable energy technologies is becoming increasingly important. Among renewable sources of energy, wind energy plays a critical role in the establishment of an environmentally sustainable low carbon economy. Globally, the majority of installed medium and large-sized wind turbines employ doubly-fed induction generators (DFIGs) to provide the variable-speed operation needed to harvest wind energy. In general, the DFIGs available on the market are standard machines which may not be the best option for a specific site. These machines tend to be large and prone to faults, and thus they need to be repaired or rewound when they fail. Currently, the common practice in the machine repair industry is to return to the original machine design as close as possible. As a consequence, a unique opportunity of redesigning the failed machines is wasted [1].

This study takes a different view by optimizing the DFIG machine design at the rewinding stage, based on an in-depth understanding of the site-specific information (i.e., wind profile) and the machine's previous performance (i.e., maximum efficiency and operating points). In this case, only the stator and rotor windings are the refinement parameters as they are the components to be replaced during the rewinding process. For large DFIG machines, a small improvement in efficiency will lead to a significant energy saving and environment benefits [1]. In the European Union, a 3% increase in the energy efficiency of electrical machines would produce electricity savings of over $2 billion per year [2]. As a result, the economic implication is also significant when improving machine design for wind turbine applications.

In fact, the optimization of machine design is a multivariable and multimodal problem [3]. Thus, the multiphysics dimension of electrical machines should be taken into account. The conventional design optimization of DFIGs relies on analytical and empirical methods. With the development of computing techniques and numerical methods, the mainstream design optimization is now based on finite element method (FEM). Accurate FEM models can facilitate the exploration of alternative designs and reduce the resource and time in both design and repair stages. However, there are two challenges.

1) A high-fidelity FEM model is lengthy and complicated to process; it may take hundreds of iterations to arrive a solution.
2) Multiple variable and constraint functions are solved simultaneously while FEM is not suitable for local sensitivity calculations, which are crucial for general gradient-based optimization.

In contrast, a surrogate modeling technique is widely used [4] to formulate an explicit relationship between the objective/constraint functions and design variables so as to reduce the FEM computational time. Furthermore, statistical methods are also useful to investigate the correlation between input parameters and numerical simulation outputs to identify significant parameters for an efficient optimal design. The obtained surrogate model can be easily used to evaluate the performance at trial design points.

It is well known that wind speed at a given installation site can vary significantly and are difficult to predict with accuracy. It is of particular importance to comprehend the distribution of wind speed frequency. At present, the Weibull model is popular because of its accuracy and easiness [5], [6]. However, the

Manuscript received June 2, 2014; revised November 28, 2014; accepted March 2, 2015. Date of publication April 1, 2015; date of current version August 18, 2015. This work was supported by the EPSRC (EP/K008552/2) and the European Commission under the Seventh Framework Programme (627270 and 318925). Paper no. TEC-00393-2014.

Z. Tan and Z. Liu are with Newcastle University, Tyne and Wear NE1 7RU, U.K. (e-mail: zheng.tan@newcastle.ac.uk; z.liu6@newcastle.ac.uk).

X. Song is with the Department of Mechanical Engineering, Dalian University of Technology, Dalian 116024, China (e-mail: sxg@dlut.edu.cn).

W. Cao is with Queen's University Belfast, Belfast BT7 1NN, U.K. (e-mail: w.cao@qub.ac.uk).

Y. Tong is with Beijing Jiao Tong University, Beijing 100044, China (e-mail: ybtong@bjtu.edu.cn).

Color versions of one or more of the figures in this paper are available online at http://ieeexplore.ieee.org.

Digital Object Identifier 10.1109/TEC.2015.2411153

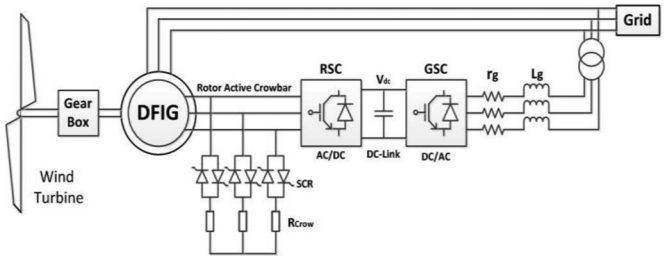

Fig. 1. Schematic of a DFIG wind turbine system.

power losses in wind turbine generators are not considered when calculating the output power of wind turbines.

This paper presents a new method based on FEM analysis, surrogate optimization and wind speed distribution for the optimal design of a DFIG in terms of maximum power output. A set of FEM models are first developed to estimate the power output of the DFIG under the characterized distribution of wind speeds at a specific site. Second, a surrogate model is constructed to approximate the input-output model and refine the machine design. Finally, the optimized design is verified by numerical and experimental tests.

II. Wind Turbine Model

A schematic diagram of the DFIG wind turbine system is shown in Fig. 1. The wind turbine is connected to the DFIG rotor through a drivetrain system, which contains high and low speed shafts, bearings and gearboxes. The DFIG is constructed from a wound rotor induction machine where its stator is directly connected to the grid and its rotor is fed by bidirectional voltage-source converters, which are two four-quadrant IGBT pulse width modulation (PWM) converters [i.e., rotor side converter (RSC) and stator side converter (GSC)] connected back-to-back by a dc-link capacitor [7]. The crowbar is used to short-circuit the RSC in order to protect the RSC from overcurrents in the rotor circuit during transient disturbances [8]. The speed and torque can be regulated by controlling the RSC.

A. Wind Energy Estimation

It is possible to characterize a wind turbine power curve based on available wind energy and the rotor power coefficient, C_p. In general, C_p can be expressed as a function of the tip speed ratio λ, which is defined by

$$\lambda = \frac{\omega R}{U} \tag{1}$$

where ω is the angular speed of the wind turbine rotor, R is the radius of the wind rotor, and U is the wind speed. For a wind turbine, C_p is represented by a nonlinear curve in terms of λ and the pitch angle β [9]

$$C_p = (0.44 - 0.0167\beta)\sin\left(\frac{\pi(\lambda - 2)}{13 - 0.3\beta}\right) - 0.00184(\lambda - 2)\beta. \tag{2}$$

Therefore, the average wind machine power is found by

$$\overline{P_w} = \frac{1}{2}\rho\pi R^2\eta\int_0^\infty C_p(\lambda)U^3 p(U)dU \tag{3}$$

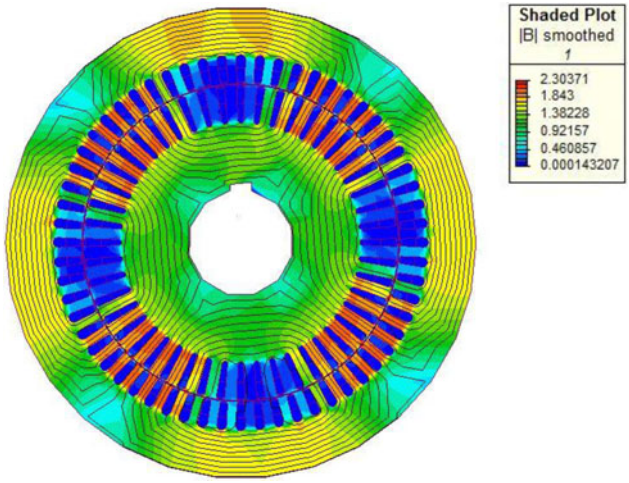

Fig. 2. Magnetic flux distribution of the DFIG at no load condition.

where ρ is the air density, η is the drive train efficiency (generator power/rotor power). In practice, wind turbine is controlled to operate at a maximum power output.

B. DFIG Mathematical Model

The DFIG model in the *d-q* reference frame is given by

$$V_{ds} = R_s i_{ds} + \frac{d\psi_{ds}}{dt} - \omega_s\psi_{qs} \tag{4}$$

$$V_{qs} = R_s i_{qs} + \frac{d\psi_{qs}}{dt} + \omega_s\psi_{ds} \tag{5}$$

$$V_{dr} = R_r i_{dr} + \frac{d\psi_{dr}}{dt} - (\omega - \omega_r)\psi_{qr} \tag{6}$$

$$V_{qr} = R_r i_{qr} + \frac{d\psi_{qr}}{dt} - (\omega - \omega_r)\psi_{dr} \tag{7}$$

$$\psi_{ds} = (L_{ls} + L_m)i_{ds} + L_m i_{dr} \tag{8}$$

$$\psi_{qs} = (L_{ls} + L_m)i_{qs} + L_m i_{qr} \tag{9}$$

$$\psi_{dr} = (L_{lr} + L_m)i_{dr} + L_m i_{ds} \tag{10}$$

$$\psi_{qr} = (L_{lr} + L_m)i_{qr} + L_m i_{qs} \tag{11}$$

where V_{ds} and V_{qs} are the *d*- and *q*-axis stator voltages; V_{dr} and V_{qr} are the *d*- and *q*-axis rotor voltages; i_{ds} and i_{qs} are the *d*- and *q*-axis stator currents; i_{dr} and i_{qr} are the *d*- and *q*-axis rotor currents, respectively. *Rs* and R_r are the phase resistances of the stator and rotor; L_{ls} and L_{lr} are the leakage inductances of the stator and rotor; L_m is the magnetizing inductance; ω_s and ω_r are the synchronous speed and the rotor speed of the DFIG, respectively.

C. Finite Element Model

A 2-D model of DFIG is built by the FE software *Infolytica MagNet*, as shown in Fig. 2. Its ratings are listed in Table I. In this model, the skin effect was ignored. The finite element model of DFIG is given by [10]

$$\frac{\partial}{\partial x}\left(v\frac{\partial A_Z}{\partial x}\right) + \frac{\partial}{\partial y}\left(v\frac{\partial A_Z}{\partial y}\right) = -J_Z$$
$$A_Z = A_{Z0} \tag{12}$$

TABLE I
MACHINE RATINGS

Parameter	Value
Rated power (kW)	55
Pole number	4
Rated speed (r/min)	1457
Stator voltage (V)	380
Stator current (A)	104
Rotor voltage (V)	394
Frequency (Hz)	50

where A_Z is the axial components of the magnetic vector potential; J_Z is the source current density; v is the material relativity; A_{Z0} is the given values for the boundary τ. It is well known that the permeability of ferromagnetic materials is much greater than that of air so that the magnetic field lines are parallel to the boundary, i.e., $A_Z = A_{Z0}$.

Based on the numerical model, the iron loss can be calculated, making it is easier to focus on the winding design (material and size).

III. WIND SPEED DATA ANALYSIS

Actual wind speed data from a U.K. wind farm at Albemarle is analyzed by statistical methods to derive the wind speed probability density function. In the literature, the Pearson model, Rayleigh model and Weibull model are widely used to fit the distribution of wind speed frequency. However, it is found from a large number of measured data that the two-parameter Weibull distribution is a good representation of the wind speed [11] and thus adopted in this paper.

A. Weibull Model

Using the Weibull model, it is very accurate to analyze the wind speed data based on the shape factor k and the scale factor c. The Weibull probability distribution function is obtained by

$$F(v) = \int_0^{+\infty} f(v)dv = 1 - e^{-\left(\frac{v}{c}\right)^k} \tag{13}$$

where v is the wind speed and the probability density is

$$f(v) = \frac{k}{c}\left(\frac{v}{c}\right)^{k-1} e^{-\left(\frac{v}{c}\right)^k}, v > 0, k, c > 0. \tag{14}$$

B. Statistic Estimation Method (SEM)

In order to estimate the Weibull probability density function, the SEM is first used to analyze the wind speed data in terms of the wind average velocity $\overline{v}$ and the standard deviation σ. $\overline{v}$ can reflect the main tendency of data change and σ represents the extent of deviation from the mean [5].
$\overline{v}$ and σ are given by

$$\overline{v} = \left(\frac{\sum_{i=1}^{n} v_i^3}{n}\right)^{\frac{1}{3}} \tag{15}$$

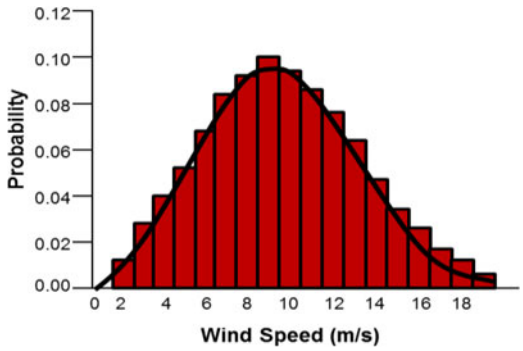

Fig. 3. Measured wind profile and its Weibull distribution.

$$\sigma^2 = \frac{1}{2}\sum_{i=1}^{n}(v_i - \overline{v})^2. \tag{16}$$

k and c can be expressed as

$$k = \left(\frac{\sigma}{\overline{v}}\right)^{-1.086} \tag{17}$$

$$c = \frac{\mu}{\Gamma\left(1 + \frac{1}{k}\right)}. \tag{18}$$

However, it is quite complex to solve the Gamma function directly. Instead, these formulas are often solved by the empirical approach [12]

$$\Gamma\left(1 + \frac{1}{k}\right) = \left(0.568 + \frac{0.434}{k}\right)^{\frac{1}{k}}. \tag{19}$$

As a result, the mean wind speed can be calculated by

$$\overline{v} = c * \Gamma\left(1 + \frac{1}{k}\right). \tag{20}$$

Following this procedure, the Weibull distribution for this wind farm is analyzed and presented in Fig. 3. A good fit can be found when compared with measured wind speed data.

IV. PROPOSED OPTIMIZATION ALGORITHM

The surrogate-based analysis and optimization is an effective tool for the design and optimization of computationally expensive models, and is widely used for airfoil shape optimization, mechanical structure and so forth. Typically, surrogate models can be comprehended as a nonlinear inverse problem, which is to determine a continuous function f of a set of design variables from a limited amount of available data **f**. But model estimation and error assessment are difficult. In this case, the predicted formula for the FEM output is $f_p(x) = \hat{f}(x) + \varepsilon(x)$. In this paper, the Kriging model [13] is adopted to create a surrogate model and a nongradient heuristic search method [14] is used to analyze calculated data by the deterministic algorithm. The proposed optimization algorithm is shown as a flowchart in Fig. 4 and is further explained in four steps.

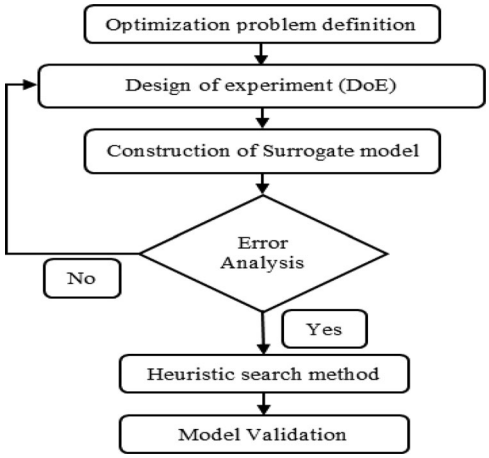

Fig. 4. Procedure of applying the surrogate modeling method.

A. Step 1—Design of Experiment (DoE)

The DoE is a sampling plan in the design variable space [14], which is aimed at maximizing the amount of information acquired and minimizing the bias error. At certain sampling points, there is a clear tradeoff between the number of points selected and the amount of information that can be extracted from these points. Due to the computational resource, the number of sample points is limited severely. On the other hand, the balance between bias and variance errors shall be found during the construction of the surrogate model. Generally, the bias error can be reduced through a DOE by distributing the sample points uniformly in the design space.

One of the most popular DoE for uniform sample distribution is Latin hypercube sampling (LHS) [15]. For arranging *p* samples with *n* design variables by LHS, the range of each parameter will be divided into *p* bins, so that the total number of p^n bins will be generated in the design space. The samples are randomly selected in the design space, and each sample will be set randomly inside a bin. Moreover, there is exactly one sample in each bin for all one dimensional projections of the *p* samples and bins. While LHS represents an improvement over unrestricted stratified sampling [16], it can provide sampling plans with very different performance. In this paper, the LHS approach is adopted. An LHS realization of 18 samples for stator windings with two design variables ($n_s = 2$) and 20 samples for rotor windings with two design variables ($n_r = 2$). Both rotor windings and stator windings have an impact on the machine performance, so an LHS realization of 56 samples for stator and rotor windings with four design variables ($n_{s\&r} = 4$).

Furthermore, the slot filling factor is one of the limit factors in winding design. Typically, it depends on the insulation thickness around the conductors and the slot, as well as the conductor shape. So this limitation shall be included into the LHS design.

B. Step 2—Numerical Simulation at Sampling Points

It is easily found that winding length and size impact on the winding resistance. In this paper, the multivariable optimization issue should consider four variables: stator winding turns, stator winding cross-sectional area, rotor winding turns, and rotor winding cross-sectional area. Among the LHS samples, if their output torque is similar, the sample with a higher efficiency is selected.

C. Step 3—Construction of the Surrogate Model

Normally, there are two surrogate model construction methods: parametric (e.g., polynomial regression, Kriging model) and nonparametric (e.g., projection pursuit regression, radial basis function) methods. The former assumes the relative global functional form between the response variable and the design variable is known while the latter constructs the whole model by using local models in different data regions.

In recent years, Kriging models are popular in dealing with computationally expensive engineering problems [17], [18], and is employed in this study. In the Kriging model, an approximation expression is given by

$$y(t) = \beta + z(t) \tag{21}$$

where β is a constant, and $z(t)$ is calculated by Gaussian distribution whose mean and variance are *0* and σ^2, respectively. If $\hat{y}(t)$ is defined as the approximation model, and the mean-squared error of $y(t)$ and $\hat{y}(t)$ are minimum, satisfying the unbiased condition. $y(t)$ is estimated as

$$\hat{f}(\mathbf{t}) = \hat{\beta} + \mathbf{r}^T(\mathbf{t})\mathbf{R}^{-1}(\mathbf{y} - \hat{\beta}\,\mathbf{q}) \tag{22}$$

where $\mathbf{R}^{-1}$ is the inverse of the correlation matrix ***R***, ***r*** is the correlation vector, *y* is *ns* observed data vector, and ***q*** is the unit vector. The correlation matrix and correlation vector are

$$R(\mathbf{t}^j, \mathbf{t}^k) = \operatorname{Exp}\left[-\sum_{i=1}^{n} \theta_i \left| t_i^j - t_i^k \right|^2\right]$$
$$(j = 1, \ldots, ns, k = 1, \ldots, ns)$$
$$\mathbf{r}(\mathbf{t}) = \left[R(\mathbf{t}, \mathbf{t}^{(1)}), R(\mathbf{t}, \mathbf{t}^{(2)}), \ldots, R(\mathbf{t}, \mathbf{t}^{(ns)})\right]^T. \tag{23}$$

The parameters $\theta_1, \theta_2, \ldots, \theta_n$ are unknown, but they can be calculated by using the following equation.

$$\text{maximize} - \frac{[n_s ln(\hat{\sigma^2}) + ln\,|\mathbf{R}|]}{2} \tag{24}$$

where $\theta_i (i = 1, 2, \ldots;, n) > 0$. θ_i can be solved by using the optimization algorithm.

D. Step 4—Particle Swarm Optimization (PSO) Algorithm

In the literature, PSO and genetic algorithm are the two prevalent evolutionary algorithms. They can be used in combination with analytical models [19] and especially the combination with FEA is gaining popularity [20], [21]. It is also suggested that PSO performs better in terms of simple implementation and high computational efficiency with few controlling parameters [22], [23] and thus used in this paper.

In an optimization case, the PSO can be described as an animal or particle moving from a certain position at random velocity in a search field. Within a population (called a swarm), each particle is treated as a point in a *d*-dimensional design space.

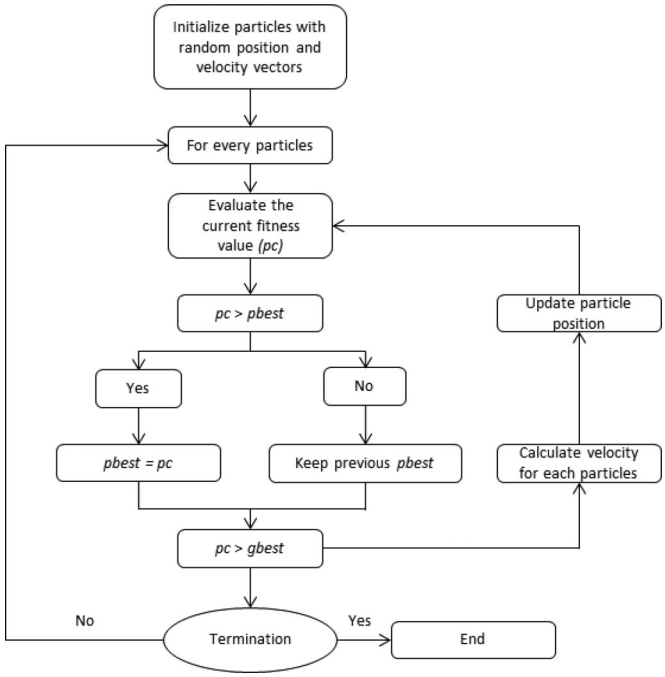

Fig. 5. PSO algorithm.

Each particle keeps track of its position in the solution space that is associated with the fitness value, termed the personal best (***pbest***). Meanwhile, there exists a global best fitness value, called global best (***gbest***). It is achieved by the whole swarm. The operation of PSO is to gradually change the velocity of each particle toward its ***pbest*** and ***gbest*** positions at each time.

The new velocity and position follow

$$V_j^{k+1} = wV_j^k + C_1\varphi_1(p_j^k - X_j^k) + C_2\varphi_2(p_g^k - X_j^k) \quad (25)$$

where V_j^k and X_j^k are the velocity and location of the *j*th particle at iteration *k*; p_j^k is the ***pbest*** of particle *j* at the *k*th iteration; p_g^k is the ***gbest*** of the entire swarm at the *k*th iteration; C_1 and C_2 are acceleration factors; φ_1 and φ_2 are the uniformly distributed random numbers between 0 and 1; *w* is the inertia weight that controls the influence of previous velocity in the new velocity. Each particle will try to change its position by four variables, which include the position of the current particle, the velocity of current particle, the distance between the current position and ***pbest***, and the distance between the current position and the ***gbest***. The PSO algorithm is illustrated in Fig. 5.

V. Numerical Tests and Results

In this paper, the optimization objective is to design winding size in order to maximize the machine efficiency as (26), by taking into account the design constraints.

$$\text{Objective}: \quad \text{Maximum} \quad \eta. \quad (26)$$

2-D variables are added to machine optimization: winding diameter *D* and winding turns *N* for rotor and stator, respectively. In total, there are six constraints: stator winding turns, stator winding diameters, rotor winding turns, rotor winding diameters, mechanical torque and fill factor. The constraints are shown in (27).

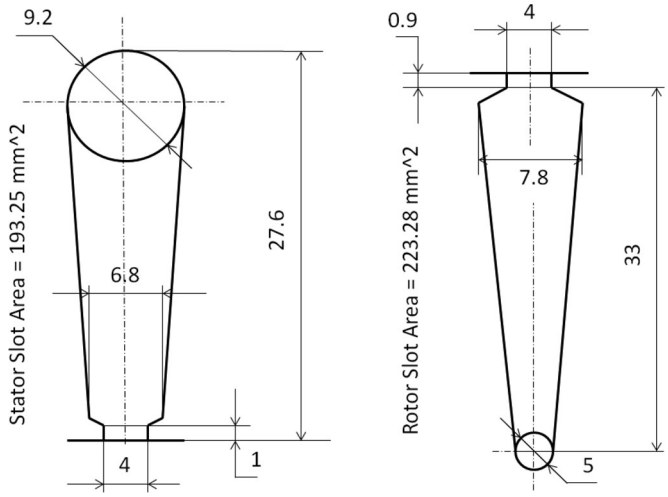

Fig. 6. Shapes of the stator and rotor slots.

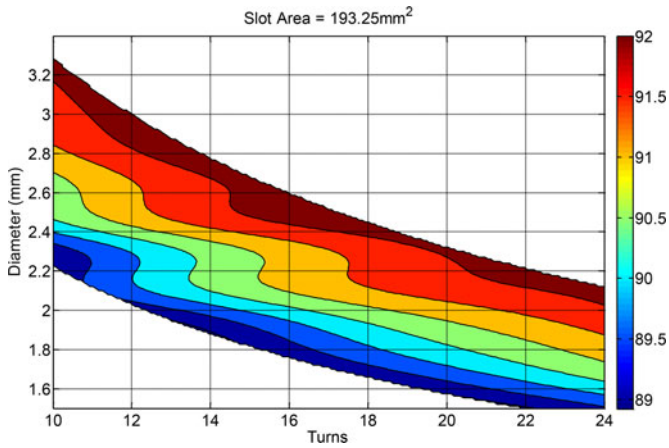

Fig. 7. Efficiency contour for stator winding optimization.

$$\begin{aligned} \text{Constraints} \quad & T \geq 360\,\text{Nm} \\ & 3.4\,\text{mm} \geq D_s \geq 1.5\,\text{mm} \\ & 3.4\,\text{mm} \geq D_r \geq 1.5\,\text{mm} \\ & 24 \geq N_s \geq 10 \\ & 24 \geq N_r \geq 10 \\ & 40\% \geq ff \geq 20\%. \end{aligned} \quad (27)$$

According to the stator and rotor slot design (see Fig. 6), the stator and rotor slot areas are calculated as 193.25 and 223.28 mm^2, respectively. Owing to the filling factor, the stator slot area of stator slot is available between 38.65 and 77.3 mm^2 while the rotor's available area is between 44.66 and 89.31 mm^2.

The test results for the 2-D variables of the stator and rotor are obtained and plotted. Fig. 7 shows the stator winding optimization function for efficiency with the 2-D variables. Fig. 8 presents the rotor winding optimization for efficiency. As can

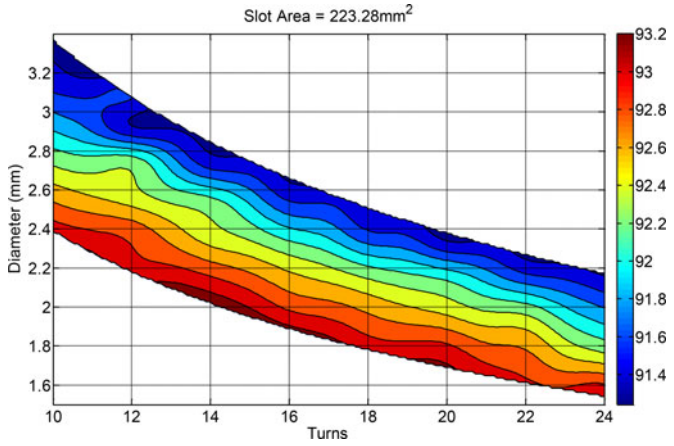

Fig. 8. Efficiency contour for rotor winding optimization.

TABLE II
ORIGINAL DESIGN

	Turns	Diameter	Torque	Efficiency
Stator	16	2.34 mm	361.89 Nm	91.61%
Rotor	12	2.97 mm		

TABLE III
OPTIMAL DESIGN OF THE STATOR WINDING

	Turns	Diameter	Torque	Efficiency
Stator	16	2.48 mm	364 Nm	92%
Rotor	12	2.97 mm		

TABLE IV
OPTIMAL DESIGN OF THE ROTOR WINDING

	Turns	Diameter	Torque	Efficiency
Stator	16	2.34 mm	361.25 Nm	91.63%
Rotor	16	2.57 mm		

TABLE V
OPTIMAL DESIGN FOR BOTH STATOR AND ROTOR WINDINGS

	Turns	Diameter	Torque	Efficiency
Stator	14	2.57 mm	361.55 Nm	92.80%
Rotor	10	2.76 mm		

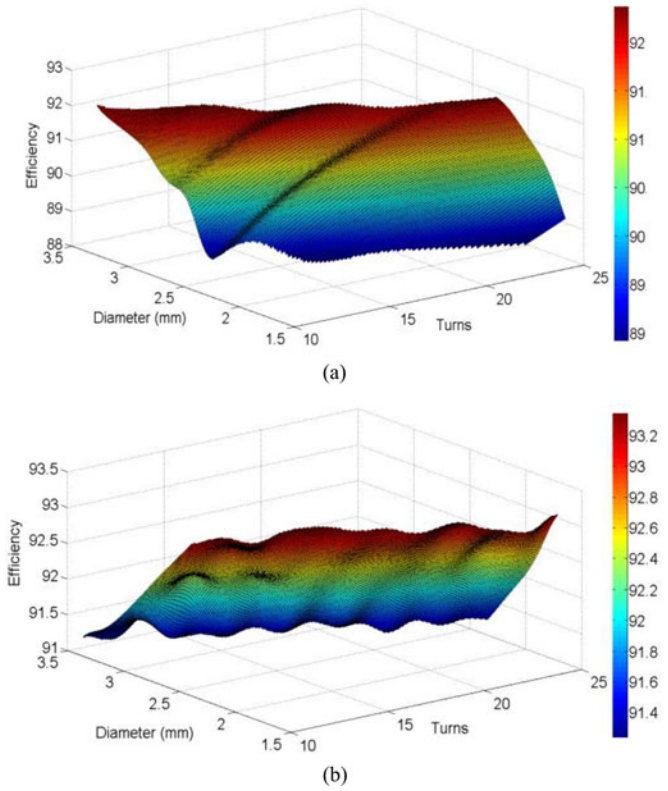

Fig. 9. Optimization of DFIG stator and rotor windings. (a) Efficiency distribution for stator winding optimization. (b) Efficiency distribution for rotor winding optimization.

TABLE VI
SUMMARY OF FINALIZED MACHINE PARAMETERS

Optimized	Parameter	Value
Yes	Stator winding cross-sectional area	5.19 mm^2
	Rotor winding cross-sectional area	5.97 mm^2
	Stator turns	14
	Rotor turns	10
No	Stator slot number	60
	Rotor slot number	48
	Winding layer	Doubly layer
	Stator winding pitch	1–14
	Rotor winding pitch	1–12
	Winding material	Copper 100% IACS
	Machine length	1150 mm
	Machine width	690 mm
	Machine height	600 mm
	Stator winding connection	2 delta
	Rotor winding connection	2 star

be seen that the local peak is optimized from the original point for both stator and rotor optimization so as to achieve maximum efficiency.

The proposed algorithm and the original plan are compared using the test function given in Tables II–V. It is clear that the proposed algorithm provides excellent results in terms of speed and accuracy. A winding design with four variables (number of turns and the diameter of both stator and rotor) is also attempted. The optimization results are visually shown in Fig. 9 and summarized in Table VI.

Having established the impacts of the stator and rotor winding parameters on the efficiency of DFIG, the results based on the rated condition can provide guidance for selecting the appreciate stator and rotor windings. However, the DFIG operates mostly between 1000 and 1457 r/min and thus the winding design should consider a wider speed range.

Fig. 10. DFIG machine test rig.

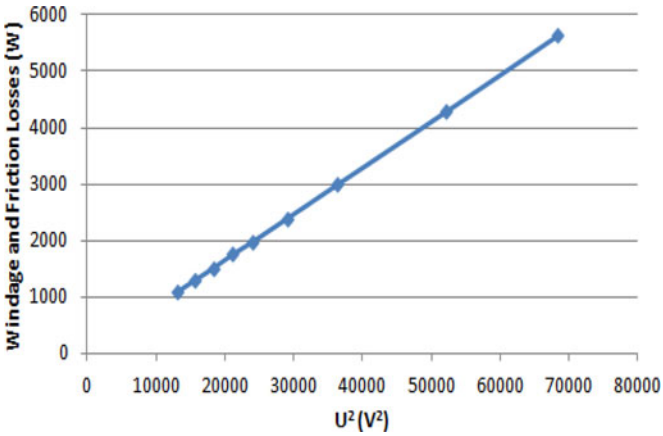

Fig. 11. Experimental results for no load test.

VI. Experimental Results and Analysis

In this paper, a 55-kW three-phase DFIG is simulated, prototyped and then tested. Its winding design with four variables (the number of turns and the diameter of both the stator and rotor) is optimized. In order to have the maximum power output at variable operating conditions, a power loss balance needs to achieve and the maximum efficiency point needs to move close to the effective operating condition [24]. Because this is a multimodal and multivariable optimization problem, it can generate many maximum efficiency samples. When the efficiency values are similar between these samples, the point with a higher torque is selected.

A test rig is set up for experimental validation, as shown in Fig. 10. A range of experiments are carried out on the machine including no load and load tests. Fig. 11 presents no-load test results from subtracting stator copper loss from the input power. This can be used to find the core loss, frictional and windage losses. A perfect linear curve indicates a good accuracy of the experimental setup and measuring equipment. Therefore, load tests are followed to test the machine from 100% to 50% load according to the standard procedures [25], [26]. Test results are presented in Figs. 12 and 13. Fig. 12 shows that the

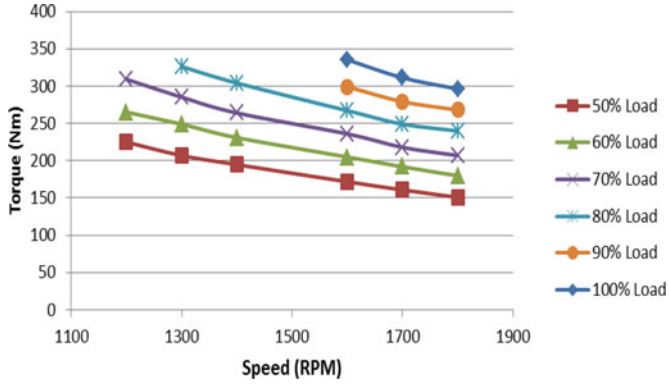

Fig. 12. Experimental results for load tests.

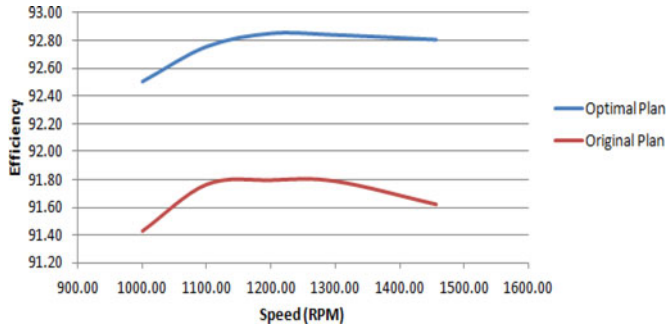

Fig. 13. Comparison between optimal and original designs.

TABLE VII
55-kW Wind Turbine Technical Data

Turbine	
Configuration	three-blade, horizontal axis
Rated power	55 kW
Cut-in wind speed	3 m/s
Rated wind speed	11 m/s
Cut-out wind speed	25 m/s
Rotor	
Rotor speed	43 r/min
Rotor diameter	19 m
Swept area	290 m^2
Power regulation	Pitch control
Hub height	19 m
Generator	
Type	DFIG
Configuration	3 Phase, 380 V, 50 Hz

experimental results agree with simulation results for the DFIG while Fig. 13 shows the improvement of approximately 1% in machine efficiency across an operational range than the original design.

Next, the prototype DFIG is used to calculate the power output under a field condition to match the specific site. This is achieved by applying the Weibull function of wind power at Albemarle. The detailed data are shown in Tables VII and VIII, and the wind turbine power curve is presented in Fig. 14. Because this wind turbine adopts the pitch-regulated control, the maximum power output is capped at 55 kW.

TABLE VIII
WIND TURBINE POWER OUTPUT

Wind Speed (m/s)	Power Output (kW)
1	0.0
2	0.0
3	0.0
4	1.1
5	4.2
6	9.2
7	15.6
8	25.1
9	36.3
10	47.9
11	55.0
12	55.0
13	55.0
14	55.0
15	55.0
16	55.0
17	55.0
18	55.0
19	55.0
20	55.0
21	55.0
22	55.0
23	55.0
24	55.0

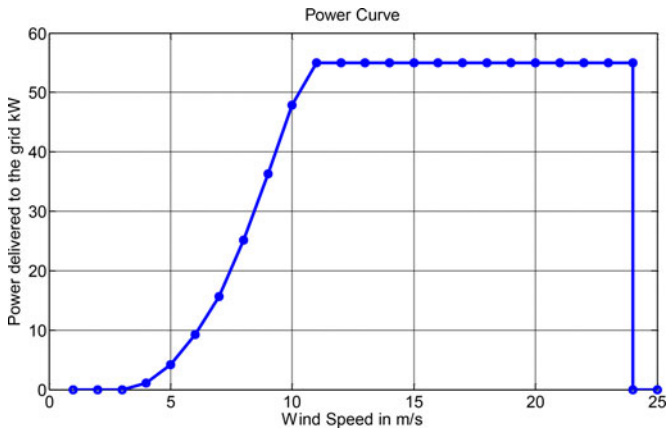

Fig. 14. Wind turbine power output curve.

For a given Weibull probability density function (site-specific), a wind turbine power curve can be attained, and so is the annual energy production. Based on the wind speed data and machine performance, the annual wind energy output at the given wind profile can be found to be approximately 63 MWh, as shown in Table IX. Compared to the original design of the DFIG, the machine efficiency is improved by 1%. In that case, the annual yield increases by about 600 kWh.

VII. CONCLUSION

A surrogate-model-based optimization of a DFIG winding design for maximizing output power has been presented. The machine is matched with a specific site taking account of the actual wind profile and the machine's operational conditions. The particle swarm optimization-based surrogate modeling techniques

TABLE IX
ANNUAL WIND POWER OUTPUT

Wind speed (m/s)	Wind energy output (kWh)
1	0.0
2	0.0
3	0.0
4	82.77
5	434.42
6	1196.73
7	2366.61
8	4273.64
9	6391.81
10	8299.85
11	8963.79
12	7949.80
13	6721.88
14	5387.29
15	3689.05
16	3020.02
17	1879.21
18	1442.61
19	1103.32
Total	63 203.80

are used in conjunction with the FEM to optimize the machine. The key refinement parameters are the stator and rotor winding windings for they are renewed during the repair and rewinding procedure.

A 55-kW DFIG is simulated and experimentally tested to check the effectiveness of the proposed techniques. No-load and load tests have confirmed the numerical and analytical machine models. The further work will extend to design and test two large DFIGs which undergo repeated repairs.

REFERENCES

[1] W. Cao, K. J. Bradley, and J. Allen, "Evaluation of additional loss in induction motors consequent on repair and rewinding," *IEE Proc. Elect. Power Appl.*, vol. 153, no. 1, pp. 1–6, Jan. 2006.
[2] A. T. De Almida and P. Fonseca, "Characterisation of EU motor use," in *Proc. Conf. Energy Efficiency Motor Drive Syst.*, pp. 143–167, 2000.
[3] J. S. Ro, C. H. Lee, and H. K. Jung, "Optimal design of ultrasonic motor using evolution strategy and finite element method," *Int. J. Appl. Electromagn. Mech.*, vol. 25, no. 1, pp. 699–704, Jul. 2007.
[4] Y. Mack, T. Goel, W. Shyy, and R. Haftka, "Surrogate model-based optimization framework: A case study in aerospace design," *Study Comput. Intell.*, vol. 51, pp. 323–342, 2007.
[5] W. Duan, J. Chen, and H. Feng, "Comparative research on methods of calculating Weibull distribution parameters of wind speed," in *Proc. Conf. Power Energy Eng.*, 2011, pp. 1–4.
[6] J. L. Acosta and S. Djokic, "Assessment of renewable wind resources in UK urban areas," in *Proc. 15th IEEE Mediterranean Electrotech. Conf.*, 2010, pp. 1439–1444.
[7] R. Pena, J. C. Clare, and G. M. Asher, "Doubly fed induction generator using back-to-back PWM converters and its application to variable speed wind-energy generation," *Proc. Inst. Elect. Eng.*, vol. 143, no. 3, pp. 231–241, May 1996.
[8] A. Petersson, L. Harnefors, and T. Thiringer, "Evaluation of current control methods for wind turbines using doubly-fed induction machines," *IEEE Trans. Power Electron.*, vol. 20, no. 1, pp. 227–235, Jan. 2005.
[9] P. Kundur, N. J. Balu, and M. G. Lauby, *Power System Stability and Control*. New York, NY, USA: McGraw-Hill, 1994.
[10] J. Li and X. Wang, "FEM analysis on interturn fault of rotor winding in DFIG," in *Proc. Int. Conf. Elect. Mach. Syst.*, Oct. 2013, pp. 797–802.
[11] M. Ding, W. Wei, and H. Wu, "Forecast wind speed probability distribution parameters and application," *Elect. Netw. Technol.*, vol. 32, no. 14, pp. 10–14, 2008.

[12] Z. Wu, "Study of wind turbine preliminary conditions in the low wind speed," M.Sc. thesis, Dept. Mech. Electron. Eng., North China Elect. Power Univ., Beijing, China, 2008.
[13] T. W. Simpson, T. M. Maucry, J. J. Korte, and F. Mistree, "Kriging models for global approximation in simulation-based multidisciplinary design optimization," *AIAA J.*, vol. 39, no. 12, Dec. 2001, pp. 2233–2241.
[14] J. R. Swisher, P. D. Hyden, S. H. Jacobson, and L. W. Schruben, "A survey of simulation optimization techniques and procedures," in *Proc. Winter Simul. Conf.*, 2000, pp. 119–128.
[15] M. McKay, W. Conover, and R. Beckman, "A comparison of three methods for selecting values of input variables in the analysis of output from a computer code," *Technometrics*, vol. 21, pp. 239–245, 1979.
[16] M. Stein, "Large sample properties of simulations using latin hypercube sampling," *Technometrics*, vol. 29, pp. 143–151, 1987.
[17] J. D. Martin and T. W. Simpson, "A study on the use of kriging models to approximate deterministic computer models," in *Proc. Design Eng. Techn. Conf. Comput. Inf. Eng. Conf.*, Sep. 2003, pp. 567–576.
[18] G. Lei, X. M. Chen, J. G. Zhu, Y. G. Guo, W. Xu, and K. R. Shao, "Multiobjective sequential optimization method for the design of industrial electromagnetic devices," *IEEE Trans. Mag.*, vol. 48, no. 11, pp. 4538–4541, Nov. 2012.
[19] Y. Duan, R. G. Harley, and T. G. Habetler, "A useful multi-objective optimization design method for PM motors considering nonlinear material properties," in *Proc. IEEE Energy Convers. Congr. Expo.*, 2009, pp. 187–193.
[20] G. Pellegrino and F. Cupertino, "FEA-based multi-objective optimization of IPM motor design including rotor losses," in *Proc. IEEE Energy Convers. Congr. Expo.*, 2010, pp. 3659–3666.
[21] R. Wrobel and P. H. Mellor, "Particle swarm optimisation for the design of brushless permanent magnet machines," in *Proc. 41st IEEE Annu. Meeting Ind. Appl. Conf.*, 2009, pp. 1891–1897.
[22] Y. Duan and R. G. Harley, "A novel method for multiobjective design and optimization of three phase induction machines," *IEEE Trans. Ind. Appl.*, vol. 47, no. 4, pp. 1707–1715, Jul./Aug. 2011.
[23] J. Kennedy and R. Eberhart, "Particle swarm optimization," in *Proc. IEEE Int. Conf. Neural Netw.*, 1995, pp. 1942–1948.
[24] W. Cao and K. J. Bradley, "Assessing the impacts of rewind and repeated rewinds on induction motors: Is an opportunity for re-designing the machine being wasted?," *IEEE Trans. Ind. Appl.*, vol. 42, no. 4, pp. 958–964, Jul./Aug. 2006.
[25] *IEEE Standard Test Procedure for Polyphase Induction Motors and Generators (ANSI)*, IEEE Standard 112, 2004.
[26] *Amendments 1: 1995 and Amendments 2: 1996, General Requirements for Rotating Electrical Machines-Part 102: Methods for Determining Losses and Efficiency From Tests (Excluding Machines for Traction Vehicles),* IEC 34-2: 1972 (IEC 34-2A 1974) (BS EN 60034-2), 2007.

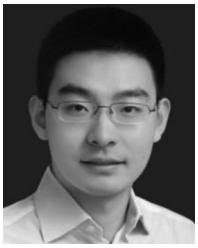

Zheng Tan (S'12) received the B.Eng. degree in electrical engineering and automation from the Inner Mongolia University of Science and Technology, Baotou, China, in 2010, and the M.Sc. degree in electrical power from Newcastle University, Newcastle upon Tyne, U.K., in 2011. He is currently working toward the Ph.D. degree in electrical machines and control at the School of Electrical and Electronic Engineering, Newcastle University.

His research interests are the doubly-fed induction generator machine design and optimization, as well as the analysis of wind power systems.

Mr. Tan received the Best Paper Award at the Linear Drives for Industry Applications (LDIA'13) Conference.

Xueguan Song (M'13) received the B.S. degree in mechanical engineering from the Dalian University of Technology, Dalian, China, in 2004, and the M.Sc. and Ph.D. degrees in mechanical engineering from Dong-A University, Busan, South Korea, in 2007 and 2010, respectively.

He is currently a Professor at the School of Mechanical Engineering, Dalian University of Technology. He has published more than 40 peer-reviewed papers, one book, and one book chapter in various research fields including engineering optimization, computational fluid dynamics analysis, thermal management, and power electronics. His research interest includes multidisciplinary design optimization, computer-aided design/computational science and optimization, and thermal management.

Dr. Song received the Best Paper Award at the Linear Drives for Industry Applications (LDIA'13) Conference, the Best Poster Awards at the Computational Science and Optimization (CSO'2011) Conference, and the Power Control and Optimization (PCO'2010) Conference, and the Honorable Mention Award from the Ph.D. Student Paper Symposium and Competition at the 2010 American Society of Mechanical Engineers- Pressure Vessels & Piping (ASME-PVP) Conference.

Wenping Cao (M'05–SM'11) received the B.Eng. degree in electrical engineering from Beijing Jiaotong University, Beijing, China, in 1991, and the Ph.D. degree in electrical machines and drives from the University of Nottingham, Nottingham, U.K., in 2004.

He is currently a Marie Curie Fellow with the Massachusetts Institute of Technology, Cambridge, MA, USA, and a Senior Lecturer with Queen's University Belfast, Belfast, U.K. His research interests are in fault analysis and condition monitoring of electric machines and power electronics.

Dr. Cao received the Best Paper Award at the Linear Drives for Industry Applications (LDIA'13) Conference, the Innovator of the Year Award from Newcastle University, in 2013, and was the Winner of the Dragons' Den Competition at Queen's University Belfast, in 2014. He is also a Member of the Institution of Engineering and Technology, and a Fellow of the Higher Education Academy. He serves as an Associate Editor for IEEE TRANSACTIONS ON INDUSTRY APPLICATIONS, IEEE INDUSTRY APPLICATIONS MAGAZINE, and *IET Power Electronics*; the Chief Editor for two special issues; and an Editor/Associate Editor for nine other international journals.

Zheng Liu (S'13) was born in Handan, China, in 1987. He received the B.S. degree in electric engineering and automation from the Huazhong University of Science and Technology, Wuhan, China, in 2009, and the M.Sc. degree in electronic and electrical engineering from the University of Sheffield, Sheffield, U.K., in 2011. He is currently working toward the Ph.D. degree at the School of Electrical and Electronic Engineering, Newcastle University, Newcastle upon Tyne, U.K.

His research interests include the multiparameter fusion-based condition monitoring technologies of electrical machines and drives.

Mr. Liu received the Best Paper Award at the Linear Drives for Industry Applications (LDIA'13) Conference.

Yibin Tong received the B.S. and M.Sc. degrees in electrical engineering from Beijing Jiaotong University, Beijing, China, in 1991 and 1998, respectively.

He is currently an Associate Professor with the School of Electrical Engineering, Beijing Jiaotong University, and a member of the National Active Distribution Network Technology Research Center, Beijing Jiaotong University. His research interests include power electronics technologies for new and renewable energy.